King Saud University

Arabian Journal of Chemistry

www.ksu.edu.sa
www.sciencedirect.com

ORIGINAL ARTICLE

CO$_2$ diffusive characteristics and influencing factors in the porous medium with saturated polyacrylamide solutions

Qingchao Cheng [a,*], Guangsheng Cao [a,*], Peilun Wang [b], Ruixuan Bu [c], Yujie Bai [a]

[a] *Key Laboratory of Enhanced Oil & Gas Recovery of Ministry of Education, Northeast Petroleum University, Daqing 163318, China*
[b] *Center of Chemistry for Frontier Technologies, Zhejiang University, Zhejiang 310028, China*
[c] *Technology Research Institute of the No. 2 Production Plant, PetroChina Daqing Oilfield Limited Company, Daqing 163461, China*

Abstract Polyacrylamide has been widely utilized to store CO$_2$ in reservoirs in order to alleviate the greenhouse impact. However, no studies have been conducted on the motion of CO$_2$ in a polyacrylamide solution within porous media. This study illustrates the effect of polyacrylamide molecular weight, concentration, pressure, temperature, and pore size on the dynamic diffusion of CO$_2$ in the core with saturated polyacrylamide solutions. The diffusion motion characteristics of CO$_2$ were obtained by diffusion experiments. The microscopic analysis of core slices following testing showed the presence of polyacrylamide on rock particles. The pressure and CO$_2$ mass fraction distribution inside the core were calculated by constructing a mathematical model. The results show that the increase in molecular weight and concentration of polyacrylamide decreased the diffusion ability of CO$_2$, while temperature and pressure accelerated the diffusion of CO$_2$. The polyacrylamide moved into the core to form an effective inhibiting effect, which was affected by CO$_2$ and pressure. While the increase in pore size accelerates the flow rate of the polyacrylamide, it also enhances the sealing capacity of the polyacrylamide solution. Scanning electron microscopy (SEM) and energy dispersive spectroscopy (EDS) showed that the core had a high content of polyacrylamide solution inside it, and these molecules were attached to the surface of the core particles in an irregular lamellar pattern. The calculation model was consistent with the diffusion experimental results, where the CO$_2$ diffusion coefficient in the polyacrylamide solution was in the order of 10^{-12} m^2/s under the

---

* Corresponding authors.
  E-mail addresses: nepu_cheng@163.com (Q. Cheng), nepucgswz@163.com (G. Cao).
Peer review under responsibility of King Saud University.

Production and hosting by Elsevier

conditions of 5–30 MPa, 323–343 K, and a core permeability of $60 \times 10^{-3} \ \mu m^2$. The results of this paper provide a new calculation for evaluating the performance of polymer plugging.

1. Introduction

Since the 1860 s to the present, the use of fossil fuels (coal, oil, and natural gas) has played an integral role in driving socio-economic development (Fizaine et al., 2016). As for the negative impact, a large amount of CO_2 is emitted into the atmosphere, leading to an increase in CO_2 concentration and causing a serious greenhouse effect. Human survival is threatened by anthropogenic global warming and rising sea levels (Yuan et al., 2016). There is an urgent need to establish CO_2 emission policies and CO_2 technical solutions to mitigate the greenhouse impact. Carbon capture and storage (CCS) is one prominent approach (Bui et al., 2018; Lau et al., 2021). CCS involves the capture, compression, transport, and injection of CO_2 into large subsurface geological reservoirs (Ajayi et al, 2019). In particular, the storage of CO_2 after injection plays an important role in the whole process (Wu et al., 2020). Many scholars have conducted studies on carbon sequestration (Chen et al., 2022; Oko et al., 2015; Pickard et al., 2014; Wall et al., 2013; M'chaar et al., 2020). Louis-César Pasquier et al. (Pasquier et al., 2014) extracted thermally activated serpentine from mining residues in combination with water to perform a parameter optimization study on CO_2 fixation. The solution was in contact with the minerals, and carbonates precipitated once the solution was saturated with dissolved CO_2. After parameter optimization, batch mode tests showed that 64 wt% of Mg could be leached from the solid phase and 62.5 wt% of CO_2 could be removed from the gas phase. Mirjafari et al. (Mirjafari et al., 2007) investigated that enhanced hydration of CO_2 and accelerated precipitation of calcium carbonate by bovine carbonic anhydrase during CO_2 injection into the formation could assist in the fixation of CO_2. The rate of the hydration reaction increased as the enzyme concentration and temperature rose. The enzyme activity was not affected by the pH of the reaction environment. The activation energy and catalytic rate constants were 700.91 cal/mol and $0.65 \ s^{-1}$, respectively. Sharma et al. (Sharma et al., 2022) purified a bacterial carbonic anhydrase (CA) for the conversion of CO_2 to $CaCO_3$ from Corynebacterium flavescens. The optimal temperature and pH for purified CA were 35 °C and 7.5, respectively. However, in the process of converting CO_2 from the gas phase to carbonate, it is necessary to ensure that the CO_2 sequestration environment in the formation is not destroyed and that constant conditions are guaranteed (McGrail et al., 2017). Hydrolyzed polyacrylamide polymer gels were used in the field of CO_2 sequestration control. The 2% concentration of acrylamide monomer and 5% sodium silicate gel system compounded by Yongli Hou et al. (Hou et al., 2010) exhibited well strength, elasticity, and plugging efficiency. The high-pressure acid environment generated by CO_2 injection not only reacts with solid silicates to form silicate gels, but it also facilitates efficient polymerization, confirming the potential for the development of composite gel systems (Olajire et al., 2010). Friedmann et al. (Friedmann et al., 1999) prepared a gel system constructed from polyacrylamide polymer, acetate ester combined with surfactant that could seal a gas intensity of 15 psi/ft under supercritical CO_2 conditions in a core of $16 \times 10^{-3} \ \mu m^2$. Li et al. (Li et al., 2016) proposed a new method for selective plugging of CO_2 channels based on a CO_2-sensitive gel system using a modified polyacrylamide-methylamine-resorcinol gel system to form gels in situ, which allowed a 90% reduction in permeability at temperatures up to 90 °C in highly permeable sandstone cores ($1698.5 \times 10^{-3} \ \mu m^2$). Zhang et al. (Zhang et al., 2020) created a polyacrylamide gel from Cr(III) and phenolic resin, which was heated at 140 °C for 120 days. No synergistic effect occurred, and the strength could still be guaranteed. Jiang et al. (Jiang et al., 2019) used free radical polymerization to create a gel from acrylamide mono-

mer, crosslinker, and initiator. The gels could be formed at temperatures ranging from 80 to 150 °C, and the gel formation time could be practically adjusted. Zareie et al. (Zareie et al., 2018) studied the strength of a sol–gel system with polyacrylamide and chromium hydroacetate as cross-linking agents to achieve sealing at 90 °C and 3000 psi pressure. No leakage occurred after 330 h at 95 °C. Yao et al. (Yao et al., 2022) synthesized an inorganic–organic composite crosslinker by adjusting the ratios of Cr(III), phenolic resin, and polyacrylamide. This composite cross-linking agent could cross-link low concentrations of polyacrylamide in oilfield wastewater to obtain a weak gel system with high temperature resistance. Sun et al. (Sun et al., 2021) evaluated the sequestration efficiency of polymer gels for CO_2 and water by calculating the residual resistance coefficient and breakthrough pressure. HPAM-Cr (III) gels had high breakthrough pressure in low permeability cores. The disproportionate seepage reduction performance was more prominent in low permeability cores. The resistance of the gels to CO_2 and brine decreased significantly over multiple cycles of injection. The structural changes of polyacrylamide polymers during CO_2 flooding, as well as the degree of influence by mineralization and formation water pressure differences, were also investigated. The performance of polyacrylamide polymers under CO_2 flooding was supplemented (Sun et al., 2017). The current study has confirmed the efficacy of polyacrylamide gels for CO_2 sequestration, but no study has reported the description of the sequestration process or the evaluation method of the sequestration effect.

In this paper, the focus was on the effect of polyacrylamide solution on CO_2 diffusion without considering the properties after the addition of cross-linking agent. The diffusion process of CO_2 being plugged by a polyacrylamide solution was elaborated upon using the pressure curves of diffusion experiments and SEM microscopic images. The amount of CO_2 intrusion in the core of a saturated polyacrylamide solution was quantified by the mathematical model of CO_2 diffusion. Meanwhile, the effects of polyacrylamide molecular weight, concentration, ambient pressure, temperature, and pore size on the sealing effect were clarified. The results of this paper provide a new calculation method for evaluating the performance of polymers on CO_2 sequestration.

2. Experiment and methodology

2.1. Materials and apparatus

The partially hydrolyzed polyacrylamide used in the experiments was produced by Henan Aisen Environmental Protec-

Table 1 Core physical parameters.

Core	Core size	Permeability, $10^{-3} \ \mu m^2$	Porosity, %
#1	D 2.5 cm × 9.68 cm	64.92	10.15
#2	D 2.5 cm × 9.67 cm	61.95	10.29
#3	D 2.5 cm × 9.73 cm	62.67	9.76
#4	D 2.5 cm × 9.71 cm	61.57	10.50
#5	D 2.5 cm × 9.63 cm	60.39	9.15
#6	D 2.5 cm × 9.70 cm	60.80	9.35
#7	D 2.5 cm × 9.75 cm	60.19	9.34
#8	D 2.5 cm × 9.69 cm	60.75	9.32
#9	D 2.5 cm × 9.66 cm	63.56	10.28
#10	D 2.5 cm × 9.71 cm	61.07	9.80

tion Co., Ltd., China, using polymers with molecular weights of 12 million and 19 million, and the content was 90.6% and 89.4%, respectively. The mother solution with a concentration of 5000 ppm was prepared using polyacrylamide powder, and further dilution was carried out to prepare solutions with 800 ppm and 2000 ppm concentrations. The CO_2 with the purity of 99.9% as the diffusion phase was produced by Teng Yun Gas Co., Ltd., China. Artificial sandstone cores were used as porous media with almost identical permeability and porosity, eliminating the influence of the cores on the results. The basic physical information of the core is shown in Table 1. A high temperature-high pressure reaction kettle, a gas booster system (a pressure vessel and a booster pump), a pressure detection system, a CO_2 gas source, and a thermostat were used in experiments. The reaction kettle was equipped with an electronically controlled heating system and a fluid stirrer, which could set the temperature and ensure the constant temperature of the gas in the reactor. The pressure detection system connected to the reactor enabled accurate pressure detection during CO_2 diffusion.

2.2. CO₂ diffusion in porous media with saturated polyacrylamide solutions

The dried cores were saturated with polyacrylamide solution at different concentrations, and to reduce the effect of shear damage on the results, the experimental flow rate was controlled at 0.05 mL/min. CO_2 was injected into the vessel and pressurized to 1.5 times the experimental pressure. It was placed on a thermostat for pre-heating to ensure that the temperature reached the target conditions quickly when CO_2 was injected into the reactor. The electric heating system of the reactor was turned on, the target temperature was set, and the saturated core

was placed. The reactor injection and discharge valves were both opened, and CO_2 was injected to purge the air from the reactor. The pressure detection system was turned on, and closed the discharge valve. The CO_2 was injected at 1.5 times the target pressure value and adjusted to the experimental pressure. The pressure data was recorded. Fig. 1 shows the experimental flow. According to the principle of mass conservation, the decrease of CO_2 in the gas phase was equal to the increase of CO_2 in the polymer solution. The amount of CO_2 (ΔN_t) in the gas phase at a specific moment when it decreases from the initial state T_0 to T_i is calculated according to the gas equation, as shown in Eq. (1) (Chen et al., 2022).

$$\Delta N_t = n_0 - n_t = \frac{1}{RT}\left(\frac{p_0 v_0}{Z_0} - \frac{p_t v_t}{Z_t}\right) = \frac{(p_0 - p_t)v}{\bar{Z} RT} = \frac{\Delta p_t v}{\bar{Z} RT} \quad (1)$$

The experimental cores were cut into thin slices along the radial direction, and the adhesion state of the polyacrylamide on the pore and rock particle surfaces was observed by an FEI Quanta 250 field emission environmental scanning electron microscope manufactured by Thermo Fisher, USA. The pore surface morphology of the core was also obtained using X-ray CT scanning.

2.3. Mathematical model

Combined with physical experiments, the diffusion model of CO_2 in saturated polymer solution cores was developed. The geometry of the diffusion model is shown as the reaction kettle in Fig. 1. The Stokes-Brinkman equation was used to explain the flow velocity and pressure fluctuations of fluids in porous media, taking into account the properties of fluid diffusion variation in permeable columnar cores. It describes the double diffusion phenomenon caused by joint heat-mass transfer. The
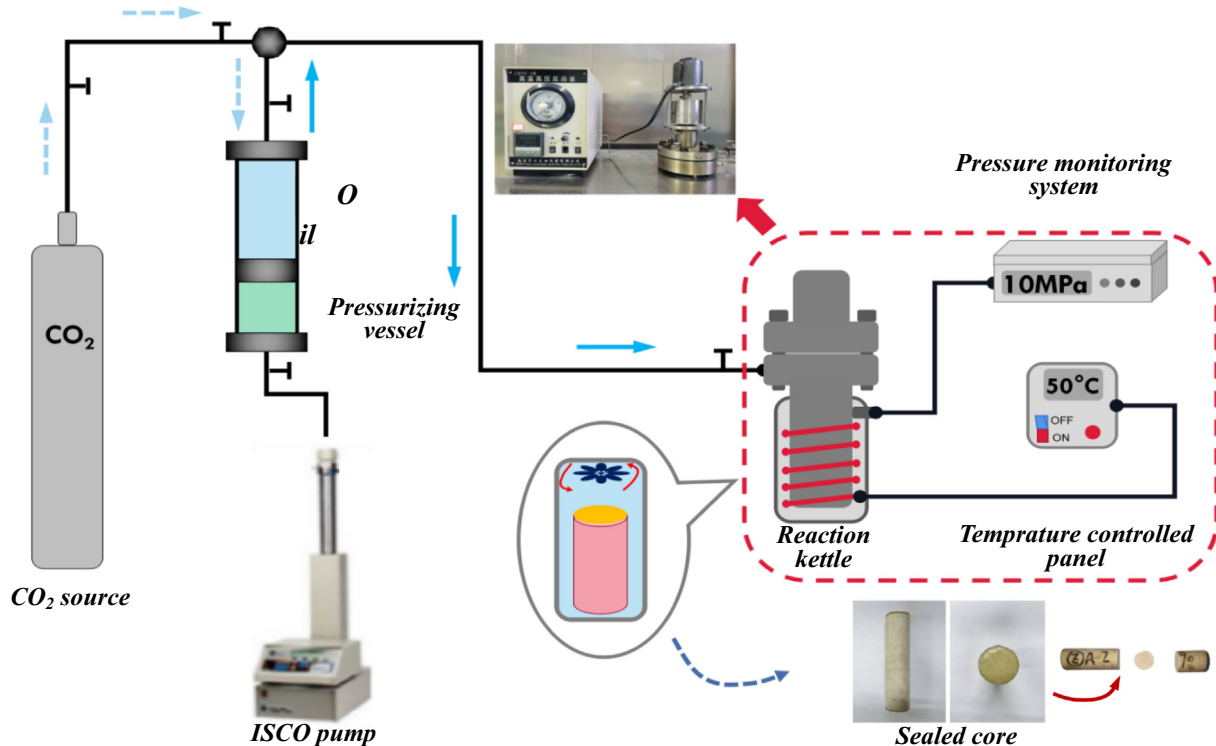

Fig. 1 Flow of CO_2 diffusion experiment.

properties of CO_2 compressibility influencing variable density were considered, and Eqs. (2), 3 were solved by the gas equation of state.

$$\frac{1}{\varepsilon}\rho\frac{\partial u}{\partial t} = \nabla \cdot [-p + K] - \left(\mu\kappa^{-1} + \beta\rho|u| + \frac{Q_m}{\varepsilon^2}\right)u$$
$$K = \mu\frac{1}{\varepsilon}\left(\nabla u + (\nabla u)^T\right) - \frac{2}{3}\mu\frac{1}{\varepsilon}(\nabla \cdot u) \quad (2)$$

$$\frac{\partial\varepsilon_p\rho}{\partial t} + \nabla \cdot (\rho u) = Q_m \quad (3)$$

Where μ is the dynamic viscosity of the fluid, kg/(m·s); u is the velocity vector, m/s; ρ is the density of the fluid, kg/m, p is the pressure, Pa;

ε is the porosity, k is the permeability of the porous medium, m^2, and the mass source, Q_m, accounts for mass deposit and mass creation within the domains. The mass exchange is assumed to occur at zero velocity. K is the viscous part of the stress. The Maxwell-Stefan diffusion model was used to describe the diffusion process of CO_2 molecules in porous media. The mass conservation equation for substance i was calculated using the Eq. (4).

$$\rho\frac{\partial\omega_i}{\partial t} + \nabla \cdot j_i + \rho(u \cdot \nabla)\omega_i = R_i \quad (4)$$

ω_i is the mass fraction of substance i, R_i is the reaction rate expression, mol/(m^3·s).

The relative mass flux within a porous medium was calculated based on the Eq. (5).

$$j_i = -\left(\rho\omega_i\sum_k\widetilde{D}_{e,ik}d_k + D_{e,i}^T\frac{\nabla T}{T}\right)D_{e,jk}$$
$$= f_e(\varepsilon_p, \tau_F)D_{ik}, D_{e,j}^T = f_e(\varepsilon_p, \tau_F)D_i^T \quad (5)$$

$\widetilde{D}_{ik}$ is the multicomponent Fick diffusion coefficient, m^2/s; d_k(SI unit: 1/m) is the driving force of diffusion, 1/m; T is the temperature, K; D_i^T is the thermal diffusion coefficient, kg/(m·s); $f_e(\varepsilon_p, \tau_F)$ is the diffusion correction factor for porous media, which is related to porosity and fluid tortuosity factor $(\tau_F = \varepsilon_p^{-1/3})$.

The diffusion driving force is defined as Eq. (6). The diffusion driving force for each substance depends on the composition, temperature and pressure of the mixture.

$$d_k = \nabla x_k + \frac{1}{p}[(x_k - \omega_k)\nabla p] \quad (6)$$

$$x_k = \frac{\omega_k}{M_k}M_n \quad (7)$$

$$M_n = \left(\sum_i\frac{\omega_i}{M_i}\right)^{-1} \quad (8)$$

M_i is the molar mass of the i; M_n is average molecular mass.

3. Results and discussion

3.1. Dynamic analysis of each diffusion step

The diffusion pressure was adjusted to 5 MPa, and the experimental temperature was 323 K in accordance with the experimental protocol in section 2.2. The dry powders of 12 million and 19 million molecular weight polyacrylamide were formulated into solutions with 800 ppm, 2000 ppm, and 5000 ppm concentrations. The results of the pressure variation of the diffusion experiment under different conditions are shown in Fig. 2.

The diffusion pressure of CO_2 in polyacrylamide solution was divided into three stages depending on the variation, which were the rapidly decreasing pressure stage (RDPS), the gradually decreasing pressure stage (GDPS), and the pressure stabilization stage (PSS). CO_2 initially contacted the exterior of the core and entered the pores of the core in unsaturated and partially saturated polymers, causing a quick reduction in pressure. After the gas was completely filled into the pores, the pressure reduction became slower, and the CO_2 molecules partially dissolved in the solution while squeezing the polyacrylamide solution, making them closer to each other, leading to a reduction in the ability of CO_2 to pass through the pores. Subsequently, the diffusion pressure was nearly smooth and the diffusion capacity was the lowest. Fig. 3 depicts the theoretical process. The amount of CO_2 diffusing into the core at each stage was quantified by the method of K-means clustering analysis based on three stages divided by pressure changes. Fig. 4 illustrates the molar mass of CO_2 diffusion at different stages. A higher percentage of CO_2
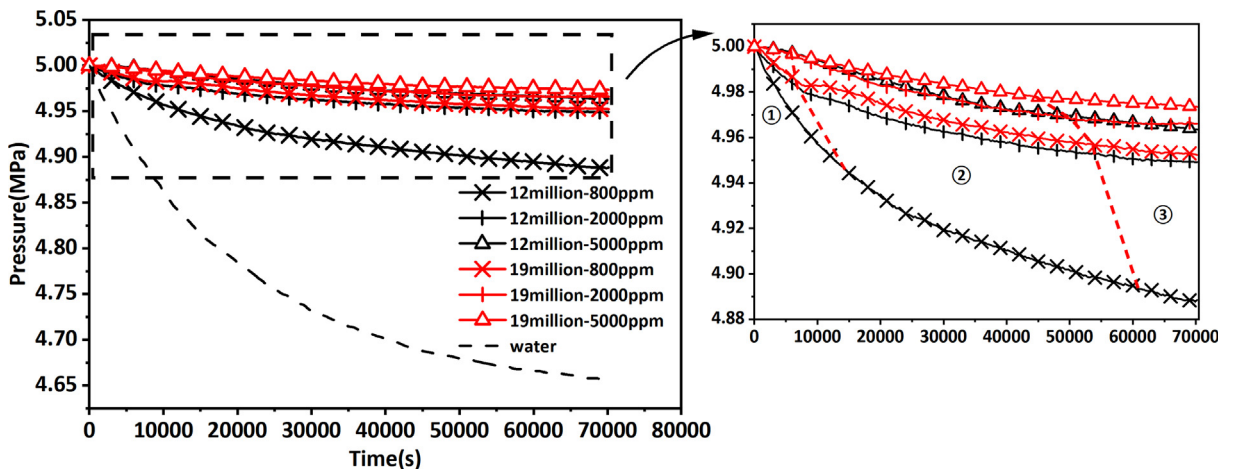

Fig. 2 Circumferential pressure variation curves of CO_2 in saturated polyacrylamide solution cores.
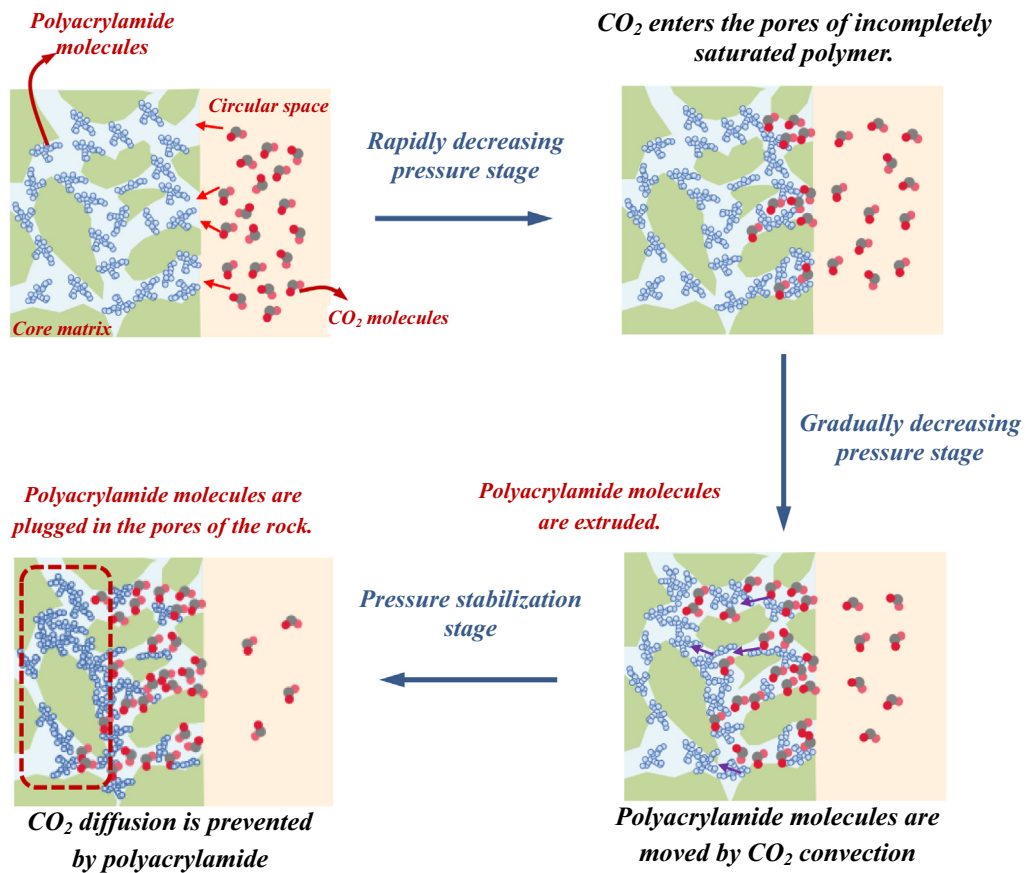
Fig. 3 Diffusion process of CO_2 in saturated polyacrylamide solution cores.

entered the core in the RDPS. The amount of CO_2 diffusion was less in the PSS.

3.2. Adhesion pattern of polyacrylamide on core particles

Cores saturated with the 12 million molecular weight, 2000 ppm concentration of polyacrylamide solution were prepared. After CO_2 diffusion experiments, the wire saw without
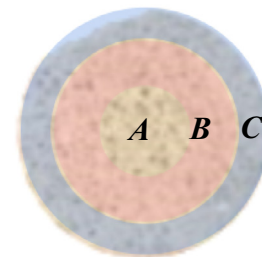

Fig. 5 The observation areas on the slice, where A is the area near the axis, B is the area in the middle of the core radius, and C is the outer area of the core.
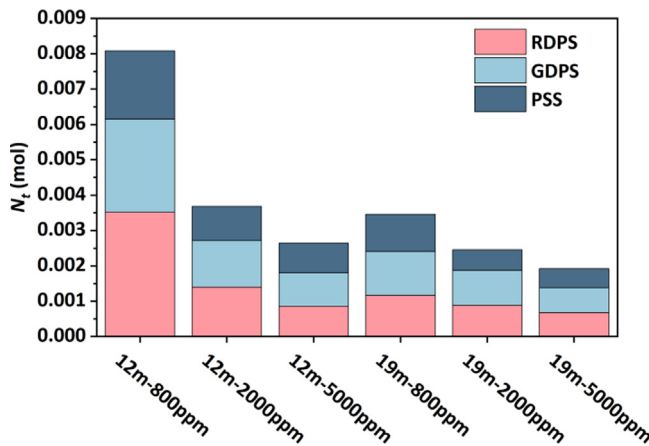
water lubrication was used in the middle of the core to cut a thin section of 3 mm thickness. SEM was used to analyze the polyacrylamide solution on the surface of the particles after lyophilization.

Fig. 5 depicts the microscopic characteristics of a three-part region along the radial direction of the core slice. Fig. 6-(a) and (b) represent the states of polyacrylamide adhesion on the rock particles near the core axis. The polyacrylamide clusters were irregularly covered on the surface, showing a lamellar pattern. The irregular polyacrylamide adhesion area was reduced on the outer side of the core (Fig. 6-(c), (d)). The amount of polyacrylamide adhesion was indicated based on the average content of carbon elements in the SEM images. The content of carbon elements radially outward along the center of the slice
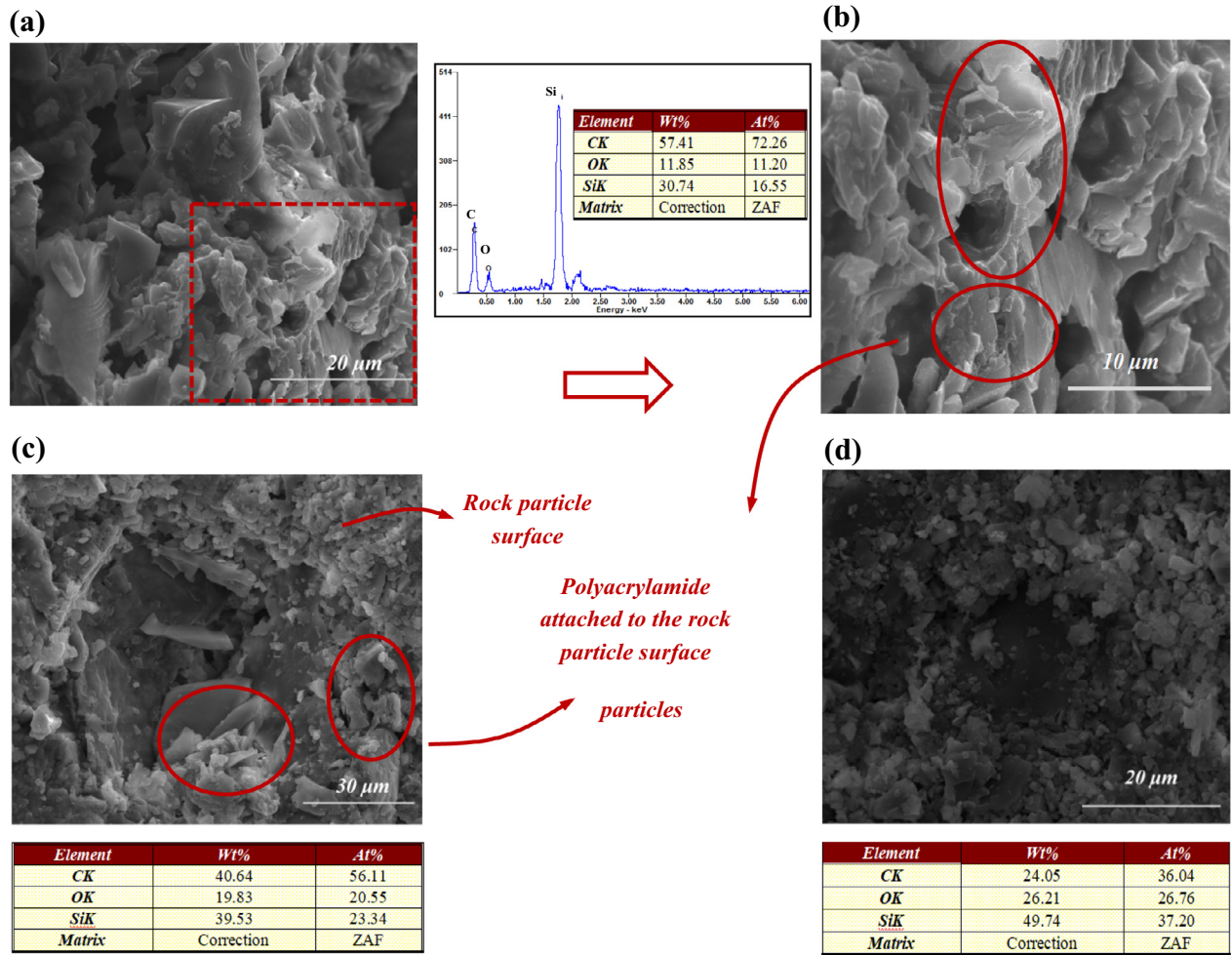

Fig. 4 Molar mass of CO_2 diffusing into the saturated core at each stages.

(a)

Element	Wt%	At%
CK	57.41	72.26
OK	11.85	11.20
SiK	30.74	16.55
Matrix	Correction	ZAF

(b)

(c)

Rock particle surface

Polyacrylamide attached to the rock particle surface

particles

Element	Wt%	At%
CK	40.64	56.11
OK	19.83	20.55
SiK	39.53	23.34
Matrix	Correction	ZAF

(d)

Element	Wt%	At%
CK	24.05	36.04
OK	26.21	26.76
SiK	49.74	37.20
Matrix	Correction	ZAF

Fig. 6 Microscopic features of different areas on the core slice. (a) is a SEM image of core area A, (b) is an enlargement of (a), (c) and (d) correspond to area B and C, respectively. Note: The data in the table are the average values of the elements at different positions in the SEM images.
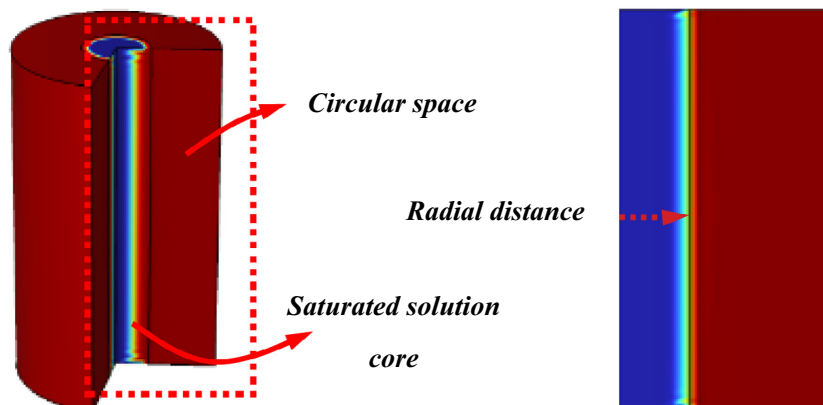

Circular space

Radial distance

Saturated solution core

Fig. 7 Geometry of the calculation model.

Table 2 Parameters of mathematical equations under initial conditions.

Mathematical equations	Parameters	Position	
		inside the core	reactor annulus
Stokes–Brinkman equation	Initial pressure	0	Setting pressure
	Dynamic viscosity	Polyacrylamide	CO_2
Maxwell–Stefan equation	Molar mass	Polyacrylamide	CO_2
	Mass fraction	Polyacrylamide concentration setting value; CO_2 mass fraction is 0	Polyacrylamide concentration is 0; CO_2 mass fraction is 1
	Diffusion coefficient	Trial value	0
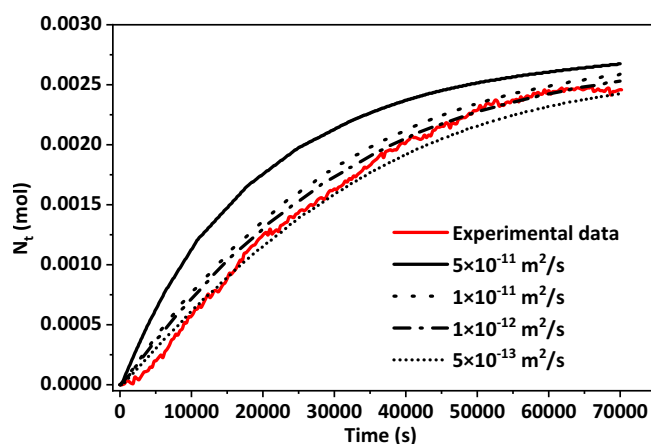
Fig. 8 Fitting of CO_2 diffusion coefficient in 19 million–2000 ppm polyacrylamide solution (323 K).

ranged from 57.41% to 24.05%. It indicated a corresponding decrease in polyacrylamide solution mass content from region A to region C.

3.3. Numerical calculation of CO_2 diffusion process

The initial conditions of the experimental process were described mathematically in Section 2.3. The initial conditions
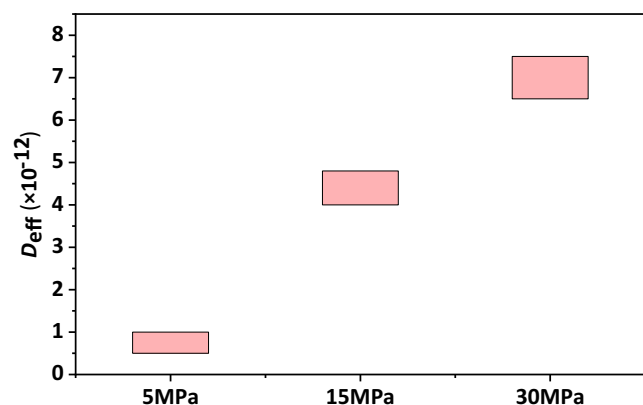
Fig. 9 CO_2 diffusion coefficients at different pressures in 19 million–2000 ppm polyacrylamide solution (323 K).

inside the core and the reactor annulus (Fig. 7) are represented in Table 2.

The mass of CO_2 entering the core increased as the diffusion coefficient increased (Fig. 8). The reaction kettle was a closed experimental environment, and the diffusion coefficient varied dynamically with the pressure. However, considering the small variation in differential pressure, the diffusion coefficient could be approximated as a constant value in the calculation process. In the process of changing the diffusion coefficient, the difference in diffusion volume was mainly reflected in the RDPS. For the 1900 million molecular weight, 2000 ppm polyacrylamide solution, the CO_2 diffusion coefficient was in the range of 5×10^{-13} to 1×10^{-12} m²/s at 5 MPa. Fig. 9 represents the calculation of the CO_2 diffusion coefficient under the condition of increasing the pressure in the reactor. As the pressure increased, the diffusion coefficient increased. In the pressure range studied at present, the diffusion coefficients were in the order of 10^{-12} m²/s.

The mass fraction of CO_2 intrusion at different locations was calculated. Fig. 10 illustrates the diffusion of CO_2 after changing the initial pressure. As the initial pressure increased, the CO_2 intrusion distance increased, although it was mostly distributed in the outside region of the core. The CO_2 mass fraction near the center of the core converged at 0.19 million–2000 ppm polyacrylamide solution, which had the effect of impeding CO_2 diffusion in the current permeability range of the core.

The intrusion distance increased from 3.5 to 7.5 mm as the pressure increased from 5 to 30 MPa, and the CO_2 mass fraction curve gradually developed an ''S'' pattern, with a smooth section at the outer edge of the core, as shown in Fig. 11. The CO_2 on the exterior of the core was close to saturation, and the saturated CO_2 mass fraction was maintained at 60% to 72%. A cliff-like decrease in CO_2 mass fraction occurred during the process toward the inner part of the core. At this stage, the polyacrylamide solution had achieved its purpose of inhibiting CO_2 diffusion, and the action range was 4–5 mm, which was the effective action area. The mass fraction of CO_2 at different locations approached smoothness as time passed, and the stability of CO_2 distribution was reached at 30,000 s.

In Fig. 12, the pressure inside the core gradually increased, and the pressure values in all parts of the core in the axial direction were consistent, while there was a slight decrease in the pressure inside the annular space. It could be seen that the higher the pressure inside the reactor, the easier the pressure variation inside the core tends to be smooth, combined
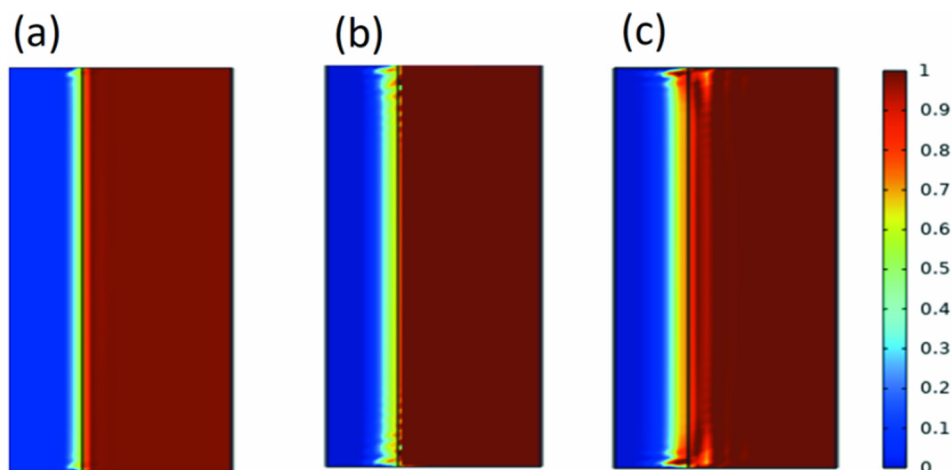
Fig. 10 CO_2 mass fraction distribution (70000 s), where the initial pressures of (a), (b), and (c) are 5 MPa, 15 MPa, and 30 MPa, respectively (323 K).

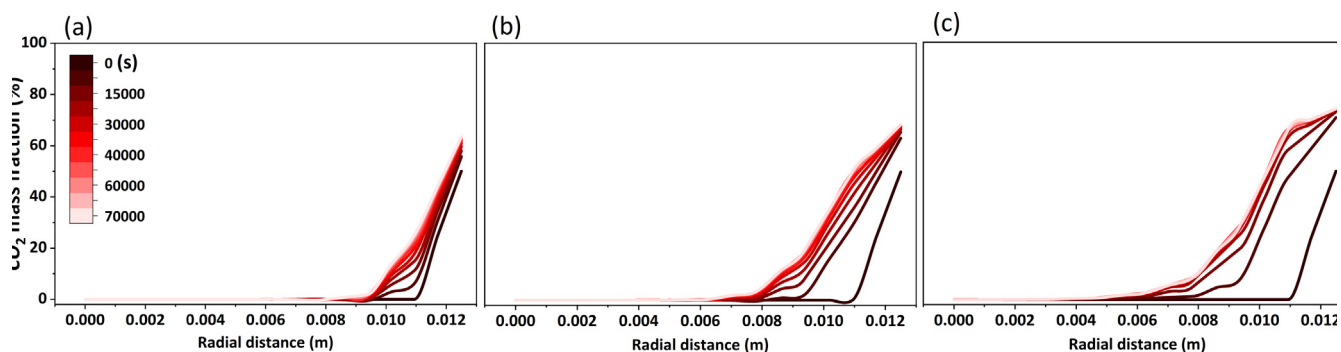**Fig. 11** CO_2 mass fraction at radial distance variation with time (323 K). The initial pressures for (a), (b), and (c) are 5 MPa, 15 MPa, and 30 MPa, respectively.
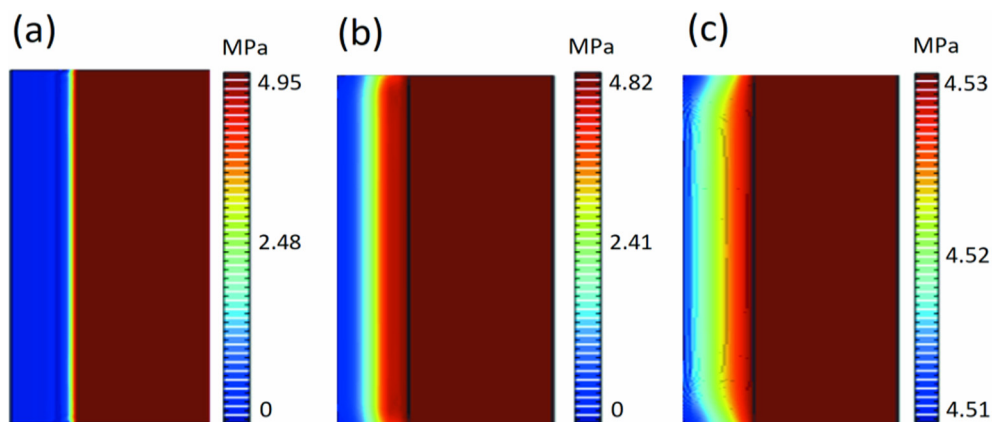

Fig. 12   Pressure variation distribution in the core, (a), (b), (c) are the pressure variation in the core at 0 s, 10000 s, and 70000 s respectively.

with the pressure variation inside the core represented in Fig. 13. The polyacrylamide solution was easily compressed, which achieved the purpose of maintaining the pressure balance inside the core. Under the current pressure conditions, the pressure inside the core reaches complete stability in 30,000–60,000 s.

3.4. Analysis of the factors influencing CO_2 diffusion

3.4.1. Effect of molecular weight and concentration of polyacrylamide on CO_2 diffusion

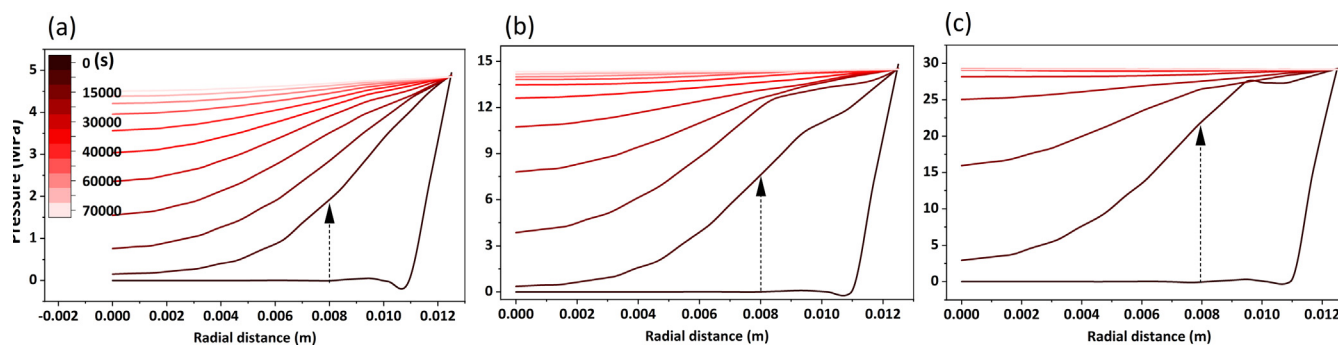The increase in molecular weight and concentration of poly-

Fig. 13 Pressure in the core along the radial distance with time (323 K). The initial pressures for (a), (b), and (c) are 5 MPa, 15 MPa, and 30 MPa, respectively.

acrylamide decreased the diffusion of CO$_2$, as shown in Fig. 2. Molecular weight and concentration exhibited the same function of impeding CO$_2$ diffusion. (12 million molecular weight–2000 ppm and 19 million molecular weight–800 ppm polyacrylamide solutions had the same inhibiting ability for CO$_2$ diffusion).

The increase in the concentration of polyacrylamide solution drastically reduced the diffusion capacity of CO$_2$. With the increase in concentration, the time of RDPS was shortened and the time of PSS was increased. When the concentration was fixed, increasing the molecular weight of polyacrylamide showed the same pattern of change.

3.4.2. Effect of temperature and pressure on CO$_2$ diffusion

Considering the cost of use and the effectiveness of inhibiting CO$_2$ diffusion, a polyacrylamide solution with the 19 million molecular weight and 2000 ppm concentration was selected for temperature and pressure tests. The effect of the change in environmental conditions on the diffusion of CO$_2$ in the polyacrylamide solution was determined.

Fig. 14 demonstrates the effect of temperature and pressure on the diffusion ability of CO$_2$ in the same saturated polyacrylamide solution core. An increase in temperature decreased the effect of polyacrylamide molecules on CO$_2$ sequestration (Fig. 14-(a)), and temperature uniformly affected the three dif-

fusion stages to a lesser extent. However, the CO$_2$ diffusion was more pronounced when compared to the initial pressure increase in the reactor (Fig. 14-(b)). During the RDPS, as the pressure increased, more CO$_2$ entered the core and reached the PSS earlier. The increase in initial pressure caused an increase in the molecular weight of CO$_2$ in the reactor compared to the increase in ambient temperature. The higher concentration difference between the inside and outside of the core elevated the rate of free molecular movement and accelerated the diffusion of CO$_2$ into the polyacrylamide solution.

3.4.3. Effect of rock pore throat size on CO$_2$ diffusion

The Fig. 15-a shows the core pore structure identified using X-ray computed tomography, and the geometric model was constructed based on the identification results. The model size was 4.2 mm × 4.2 mm × 0.3 mm, and the pore size ranges from 27 to 307 μm. At constant pressure conditions, CO$_2$ was sequestered in a rectangular area, and the pores were saturated with a 19 million molecular weight, 2000 ppm concentration polyacrylamide solution.

The size of the geometric model was adjusted separately to calculate the flow velocity of the solution and the mass concentration of CO$_2$ intrusion into the pores at 14–154 μm, 27–307 μm, 41–461 μm, 54–614 μm, 68–768 μm, and 91–921 μm pore sizes, respectively. CO$_2$ flows through the pores of satu-
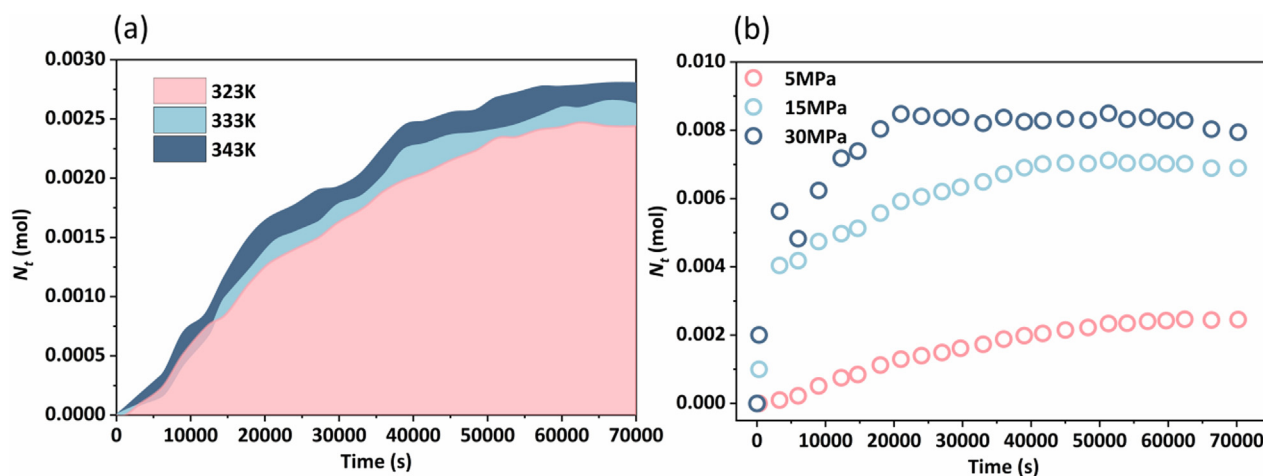

Fig. 14 CO$_2$ diffusion in polyacrylamide solution under different conditions. (a) CO$_2$ diffusion in 19 million-2000 ppm polyacrylamide solution at different temperatures (5 MPa), (b) CO$_2$ diffusion in 19 million-2000 ppm polyacrylamide solution at different pressures (323 K).
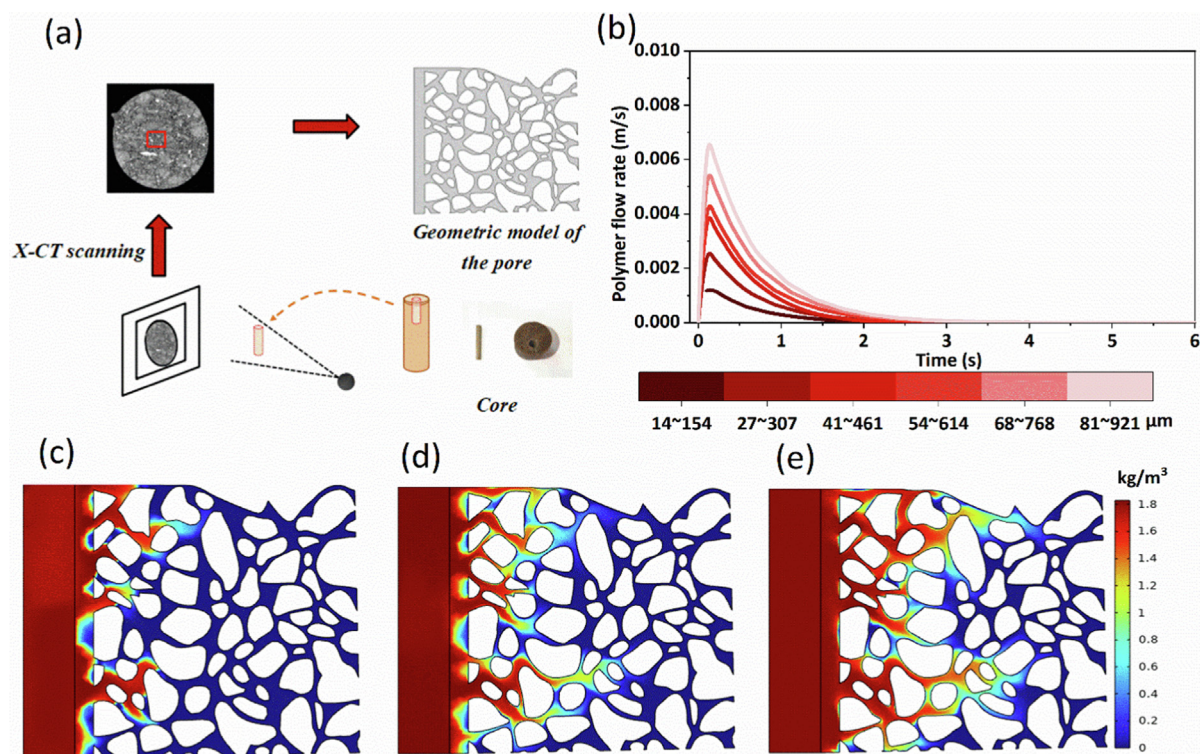
Fig. 15 CO_2 diffusion characteristics in saturated solution with different pore sizes. (a) is the pore geometry model; (b) is the polymer flow rate for different pore sizes; (c), (d), (e) are the CO_2 mass concentration distributions corresponding to 14–154 μm, 41–461 μm, and 91–921 μm pore sizes, respectively.

rated polyacrylamide solution along continuous and larger pore throat size channels, forming dominant channels (Fig. 15-c, d, and e). The large size pores were first plugged in the process of injecting polyacrylamide solution into the formation, so the purpose of plugging CO_2 was achieved. However, the polyacrylamide solution between the prominent channels had little effect on inhibiting CO_2 diffusion. Fig. 15-b represents the flow velocity of the solution for different pore sizes. Its values gradually increased with time when CO_2 was first released due to the weak compressibility of the polyacrylamide solution.

The outflow velocity reached a maximum after the polyacrylamide molecules squeezed each other. As the solution started to plug CO_2, the flow velocity decreased until it was 0. The flow velocity increased with the increase in pore size, and the peak value was reached after changing different pore sizes. However, the flow rate was faster, and its sequestration rate was accelerated.

4. Conclusions

In summary, the polyacrylamide was effective in inhibiting CO_2 under reservoir conditions. The diffusion of CO_2 in the core of a saturated polyacrylamide solution was divided into three stages depending on the degree of pressure change. The pressure data, scanning electron microscopy, and energy spectra confirmed that after CO_2 diffusion, it moved the polyacrylamide solution until plugging was achieved. The effects of molecular weight, concentration, pressure, and temperature on the dynamic diffusion of CO_2 in the core of saturated polyacrylamide molecules were clarified using diffusion experiments. Polyacrylamide solutions with molecular weights of 12 and 19 million were studied to hinder the diffusion state of CO_2 and were formulated

to 800 ppm, 2000 ppm, and 5000 ppm concentrations, respectively. The increase in molecular weight and concentration exhibited the same function of impeding CO_2 diffusion. In addition, the pressure range of this experiment was 5–30 MPa and the temperature was 323–343 K. The increase in temperature decreased the effect of polyacrylamide molecules on CO_2 sequestration, uniformly affecting the three diffusion stages. However, the initial pressure in the reactor increased, and the CO_2 diffusion was more rapid. The increase in pore size accelerated the flow rate of the polymer. The range of sizes studied can also have a sequestering effect.

The results calculated using a combination of the mathematical models correspond well to the experimental results. The CO_2 diffusion coefficient in the polyacrylamide was calculated to be on the order of 10^{-12} m²/s at a core permeability of 60×10^{-3} μm². The mass fraction and pressure of CO_2 in the core were given. The external side of the core was saturated with a CO_2 mass fraction in the range of 60% to 72%. The CO_2 mass fraction in the interior of the core was substantially reduced. The polyacrylamide achieved the purpose of plugging CO_2 diffusion. The results presented in this paper provide a new computational method to evaluate the CO_2 sequestration effect of polymers.

Declaration of Competing Interest

The authors declare that they have no known competing financial interests or personal relationships that could have appeared to influence the work reported in this paper.

Appendix A. Supplementary material

Supplementary data to this article can be found online at https://doi.org/10.1016/j.arabjc.2023.105106.

References

Ajayi, T., Gomes, J.S., Bera, A., 2019. A review of CO$_2$ storage in geological formations emphasizing modeling, monitoring and capacity estimation approaches. Pet. Sci. 16, 1028–1063. https://doi.org/10.1007/s12182-019-0340-8.

Bui, M., Fajardy, M., Mac Dowell, N., 2018. Bio-energy with carbon capture and storage (BECCS): Opportunities for performance improvement. Fuel 213, 164–175. https://doi.org/10.1016/j.fuel.2017.10.100.

Chen, H., Yang, M., Huang, C., Wang, Y., Zhang, Y., Zuo, M., 2022. A dynamic model of CO$_2$ diffusion coefficient in shale based on the whole process fitting. Chem. Eng. J. 428,. https://doi.org/10.1016/j.cej.2021.131151 131151.

Fizaine, F., Court, V., 2016. Energy expenditure, economic growth, and the minimum EROI of society. Energy Policy 95, 172–186. https://doi.org/10.1016/j.enpol.2016.04.039.

Friedmann, F., Hughes, T.L., Smith, M.E., Hild, G.P., Wilson, A., Davies, S.N., 1999. Development and testing of a foam-gel technology to improve conformance of the Rangely CO$_2$ flood. SPE Reservoir Eval. Eng. 2 (01), 4–13. https://doi.org/10.2118/54429-PA.

Hou, Y., Yue, X.A., 2010. Research on a novel composite gel system for CO$_2$ breakthrough. Pet. Sci. 7, 245–250. https://doi.org/10.1007/s12182-010-0028-6.

Jiang, G., Deng, Z., He, Y., Li, Z., Ni, X., 2019. Cross-linked polyacrylamide gel as loss circulation materials for combating lost circulation in high temperature well drilling operation. J. Pet. Sci. Eng. 181,. https://doi.org/10.1016/j.petrol.2019.106250 106250.

Lau, H.C., Ramakrishna, S., Zhang, K., Radhamani, A.V., 2021. The role of carbon capture and storage in the energy transition. Energy Fuels 35 (9), 7364–7386. https://doi.org/10.1021/acs.energyfuels.1c00032.

Li, D.X., Zhang, L., Liu, Y.M., Kang, W.L., Ren, S.R., 2016. CO$_2$-triggered gelation for mobility control and channeling blocking during CO$_2$ flooding processes. Pet. Sci. 13, 247–258. https://doi.org/10.1007/s12182-016-0090-9.

McGrail, B.P. et al, 2017. Field validation of supercritical CO$_2$ reactivity with basalts. Environ. Sci. Technol. Lett. 4 (1), 6–10. https://doi.org/10.1021/acs.estlett.6b00387.

M'chaar, R., Ouerfelli, N., Messaâdi, A., Zrelli, N., Ferreira, I.L., Hafez, B., Elmsellem, H., 2020. A simplified model correlating the excess proprieties for Bi-X binary systems (X = Cu, Sb) serving the concept of reduced Redlich-Kister function at different temperatures. Surf. Interfaces 21,. https://doi.org/10.1016/j.surfin.2020.100643 100643.

Mirjafari, P., Asghari, K., Mahinpey, N., 2007. Investigating the application of enzyme carbonic anhydrase for CO$_2$ sequestration purposes. Ind. Eng. Chem. Res. 46 (3), 921–926. https://doi.org/10.1021/ie060287u.

Oko, E., Wang, M., Olaleye, A.K., 2015. Simplification of detailed rate-based model of post-combustion CO$_2$ capture for full chain CCS integration studies. Fuel 142, 87–93. https://doi.org/10.1016/j.fuel.2014.10.083.

Olajire, A.A., 2010. CO$_2$ capture and separation technologies for end-of-pipe applications–A review. Energy 35 (6), 2610–2628. https://doi.org/10.1016/j.energy.2010.02.030.

Pasquier, L.C., Mercier, G., Blais, J.F., Cecchi, E., Kentish, S., 2014. Parameters optimization for direct flue gas CO$_2$ capture and sequestration by aqueous mineral carbonation using activated serpentinite based mining residue. Appl. Geochem. 50, 66–73. https://doi.org/10.1016/j.apgeochem.2014.08.008.

Pickard, S.C., Daood, S.S., Pourkashanian, M., Nimmo, W., 2014. Co-firing coal with biomass in oxygen-and carbon dioxide-enriched atmospheres for CCS applications. Fuel 137, 185–192. https://doi.org/10.1016/j.fuel.2014.07.078.

Sharma, T. et al, 2022. Enzyme mediated transformation of CO$_2$ into calcium carbonate using purified microbial carbonic anhydrase. Environ. Res. 212,. https://doi.org/10.1016/j.envres.2022.113538 113538.

Sun, X., Bai, B., 2017. Dehydration of polyacrylamide-based super-absorbent polymer swollen in different concentrations of brine under CO$_2$ conditions. Fuel 210, 32–40. https://doi.org/10.1016/j.fuel.2017.08.047.

Sun, X., Bai, B., Alhuraishawy, A.K., Zhu, D., 2021. Understanding the plugging performance of HPAM-Cr (III) polymer gel for CO$_2$ conformance control. SPE J. 26 (05), 3109–3118. https://doi.org/10.2118/204229-PA.

Wall, T., Stanger, R., Liu, Y., 2013. Gas cleaning challenges for coal-fired oxy-fuel technology with carbon capture and storage. Fuel 108, 85–90. https://doi.org/10.1016/j.fuel.2011.03.037.

Wu, Y., Li, P., 2020. The potential of coupled carbon storage and geothermal extraction in a CO$_2$-enhanced geothermal system: a review. Geotherm. Energy 8 (1), 1–28. https://doi.org/10.1186/s40517-020-00173-w.

Yao, E., Yu, G., Li, B., Zhao, L., Li, Y., Bai, H., Zhou, F., 2022. High-temperature-resistant, low-concentration water-controlling composite cross-linked polyacrylamide weak gel system prepared from oilfield sewage. ACS omega 7 (15), 12570–12579. https://doi.org/10.1021/acsomega.1c05675.

Yuan, Z., Eden, M.R., Gani, R., 2016. Toward the development and deployment of large-scale carbon dioxide capture and conversion processes. Ind. Eng. Chem. Res. 55 (12), 3383–3419. https://doi.org/10.1021/acs.iecr.5b03277.

Zareie, C., Sefti, M.V., Bahramian, A.R., Salehi, M.B., 2018. A polyacrylamide hydrogel for application at high temperature and salinity tolerance in temporary well plugging. Iran. Polym. J. 27, 577–587. https://doi.org/10.1007/s13726-018-0634-5.

Zhang, S., Guo, J., Gu, Y., Zhao, Q., Yang, R., Yang, Y., 2020. Polyacrylamide gel formed by Cr (III) and phenolic resin for water control in high-temperature reservoirs. J. Pet. Sci. Eng. 194,. https://doi.org/10.1016/j.petrol.2020.107423 107423.